Computers and Geotechnics 54 (2013) 192–201

Contents lists available at ScienceDirect

Computers and Geotechnics

journal homepage: www.elsevier.com/locate/compgeo

A dynamic large deformation finite element method based on mesh regeneration

D. Wang *, M.F. Randolph, D.J. White

Centre for Offshore Foundation Systems, The University of Western Australia, Australia

ARTICLE INFO

Article history:
Received 8 March 2013
Received in revised form 5 July 2013
Accepted 6 July 2013
Available online 6 August 2013

Keywords:
Large deformation
Finite element method
Clays
Penetration
Landslides
Footing

ABSTRACT

In this paper, a large deformation finite element (LDFE) approach termed 'remeshing and interpolation technique with small strain (RITSS)' is extended from static to dynamic soil-structure interaction applications. In addition, a technique termed 'element addition' is developed to improve the computational efficiency of both static and dynamic LDFE analyses that involve moving boundaries. The RITSS approach is based on frequent mesh generation to avoid element distortion. In dynamic RITSS, the field variables mapped from the old to the new mesh involve not only the stresses and material properties, but also the nodal velocities and accelerations. Using the element addition technique, new soil elements are attached to the domain boundaries periodically when the soil near the boundaries becomes affected by large displacements of the structure. The procedures of this Abaqus-based dynamic LDFE analysis and element addition technique are detailed, and the robustness of the techniques is validated and assessed through three example analyses: penetration of a flat footing into a half-space and movement of rigid and deformable landslides down slopes.

1. Introduction

Many applications in geotechnical engineering involve large movements of foundations, anchors or other elements relative to the soil. These include cone penetration, lateral buckling of partially-embedded pipelines, rotation and translation of deep anchors and run-out of landslides. Current large deformation numerical methods based on continuum mechanics can be broadly divided into two categories: finite element (FE) methods and meshless methods. Most large deformation finite element (LDFE) methods were established within the framework of a 'decoupled' arbitrary Lagrangian–Eulerian (ALE) approach to overcome mesh distortion problems. In ALE FE methods the mesh displacements and material displacements are not required to be solved simultaneously [1]. Specific applications of the ALE approach to geomechanics problems have been reported by Di et al. [4] and Nazem et al. [13], Nazem et al. [12]. Recently, Kardani et al. [8] incorporated the h-adaptive technique into the ALE approach, to improve the numerical accuracy by continuously refining the mesh in the zone of concern.

This paper describes an extension of the LDFE approach known as 'remeshing and interpolation technique with small strain' (RITSS), which has been widely used in offshore geotechnical applications [7]. Previous studies have considered shallow and deep foundations [16,21,22,19,23], penetrometers [26,27] and pipelines [24]. Essentially, the RITSS approach can also be regarded as a special decoupled ALE method. The overall scheme of the RITSS approach is to divide the displacements of the structural element into typically dozens to thousands of incremental steps. The displacements of the element in each step must be small enough to avoid gross distortion of the soil element. The Lagrangian calculation is thus performed in each step, followed by re-meshing of the deformed geometry and 'convection' of the stresses and material properties from the old mesh to the new mesh. In the RITSS approach, quadratic elements are used and it is not mandatory to retain the original mesh topology during re-meshing. A distinct advantage of the RITSS approach is that it can be coupled with most FE programs. Existing applications of the RITSS method have been built around locally developed codes such as AFENA [2] and the commercial package Abaqus.

The RITSS approach was initially proposed by Hu and Randolph [7]. Several important advances achieved during the last decade include partial remeshing techniques, expansion from two-dimensional (2D) to three-dimensional (3D) applications and implementation in coupled analysis as summarized by Randolph et al. [15]. Also, the soil constitutive model incorporated into the LDFE analyses has evolved from the simple elastic-perfectly plastic model to more complex ones, such as the modified Cam-Clay model for coupled analysis [20] and a strain-softening rate-dependent

* Corresponding author. Address: Centre for Offshore Foundation Systems, The University of Western Australia, 35 Stirling Highway, Crawley, WA 6009, Australia. Tel.: +61 8 6488 3447; fax: +61 8 6488 1044.

E-mail addresses: dong.wang@uwa.edu.au (D. Wang), mark.randolph@uwa.edu.au (M.F. Randolph), david.white@uwa.edu.au (D.J. White).

0266-352X/$ - see front matter © 2013 Elsevier Ltd. All rights reserved.
http://dx.doi.org/10.1016/j.compgeo.2013.07.005

Tresca model for total stress analysis [27,24]. The robustness of the RITSS approach has been fully verified by comparison with small strain FE methods, plasticity limit analysis solutions and experimental model tests. However, the previous RITSS applications were focused on static problems, neglecting inertial effects. Inertia may be critical in capturing the responses of soils in medium- and high-velocity processes, which include subaerial or submarine landslides, the installation of deep penetrating anchors and post-liquefaction spreading of embankments.

In this paper, an Abaqus-based RITSS approach that can be applied to dynamic geotechnical problems is presented. The approach is validated through comparison with solutions from other LDFE approaches and simplified analysis. All of the benchmark studies were limited to plane strain conditions, but the proposed strategy is also appropriate for 3D RITSS implementations and can be coupled with most standard FE packages. An element addition technique is also developed to reduce the computational effort in dynamic problems. The element addition technique is aimed at structural elements or soil masses undergoing monotonic movement involving inertial forces, but is not intended for dynamic analyses related to seismic loading.

2. Dynamic ritss approach

2.1. Governing equations and time integration

The dynamic equilibrium equation is expressed as

$$M\ddot{u} + C\dot{u} + F_{\text{int}} = F_{ext} \tag{1}$$

where M and C represent the mass and damping matrices, respectively, and u and $\dot{u}$ are the acceleration and velocity vectors. The internal force vector F_{int} depends on the current stress vector σ. F_{ext} is the external force vector, determined by the dynamic or sustained loads applied.

For each step of the dynamic RITSS analysis, Eq. (1) is solved using an implicit time integration scheme proposed by Hilber et al. [6]. This integration scheme is actually a generalised Newmark operator with controllable numerical damping. The numerical damping is to filter out high-frequency noise induced by the inability of the spatial discretisation to model high-frequency waves. The acceleration, velocity and displacements at time $(t + \Delta t)$ are calculated as [3]

$$\begin{aligned} &M\ddot{u}^{t+\Delta t} + (1+\alpha)\left(Cu^{t+\Delta t} + F_{\text{int}}^{t+\Delta t}\right) - \alpha\left(Cu^{t} + F_{\text{int}}^{t}\right) \\ &\quad = (1+\alpha)F_{ext}^{t+\Delta t} - \alpha F_{ext}^{t} \end{aligned} \tag{2}$$

$$\dot{u}^{t+\Delta t} = \dot{u}^{t} + \Delta t[(1-\theta)\ddot{u}^{t} + \theta\ddot{u}^{t+\Delta t}] \tag{3}$$

$$u^{t+\Delta t} = u^{t} + \Delta t\dot{u}^{t} + \Delta t^{2}[(0.5-\beta)u^{t} + \beta u^{t+\Delta t}] \tag{4}$$

where Δt is the time step and α, θ and β are integration parameters. The integration scheme through Eqs. (2)–(4) has second-order accuracy and unconditional stability when $-1/3 < \alpha < 0$, $\theta = 0.5 - \alpha$ and $\beta = (1 - \alpha^2)/4$. The parameter α, indicating the numerical damping introduced, was taken as -0.05 in the RITSS analyses.

The definitions of strains and stresses follow finite strain theory, to eliminate unrealistic strains induced by rigid body rotation and also to ensure rotation of the stresses with the material. In the dynamic RITSS approach an updated Lagrangian (UL) formulation is implemented using the above implicit scheme (Eqs. (2)–(4)) in each step. Correspondingly, the strains and stresses on the deformed configuration are measured with the rate of deformation and Cauchy stress, which are work conjugate. These measurements are appropriate and applicable for the elasto-plastic constitutive models that are most widely used in geotechnical numerical studies. The Jaumann rate is selected as the objective stress rate [3]. 'Small strain' in the term RITSS indicates that compared with large deformations during the entire response, the soil deformation in each step is small. As such, it is not strictly necessary to adopt the finite strain (UL) formulation for the increments between remeshing stages. However, the authors have generally adopted the UL formulation as incorporating RITSS in Abaqus (e.g. [19,24].

2.2. Procedure of dynamic large deformation analysis

In contrast to conventional small strain FE methods based on purely Lagrangian algorithms, the RITSS approach features mesh regeneration and projection of field variables. The field variables in the static total stress RITSS approach consist of the stresses and material properties. The field variables are recovered from the old integration points to each element node, and are then interpolated onto each new integration point for the next incremental solution step. The Superconvergent Patch Recovery (SPR, [28] was selected to recover field variable within a patch of elements to individual nodes:

$$V^{*} = Pa \tag{5}$$

where V^{*} represents a field variable recovered, P is a polynomial expansion and vector a comprises a finite number of unknown parameters. For 2D quadratic elements, P is written as

$$P = (1 \quad x \quad y \quad x^2 \quad y^2 \quad xy) \tag{6}$$

For an element patch with total n sampling points, the error of the recovered field variable is minimized

$$\Pi = \sum_{k=1}^{n}(\hat{V} - Pa)^2 \tag{7}$$

$$\frac{\partial \Pi}{\partial a} = 0 \tag{8}$$

where $\hat{V}$ is the FE solution at the sampling point. After the parameter vector a is deduced from Eq. (8), it is substituted into Eq. (5) to obtain the field variable at the element node.

The soil was meshed with quadratic 6-noded triangular elements. The integration points of the triangular elements were empirically found to be the optimal sampling points which exhibit one order higher convergence than for other positions. In our previous static simulations of pipe-soil interaction and plate anchor keying, the quality of SPR for triangular elements has already been validated [24,19].

The material properties extrapolated include, at least, material density and state variables for history-dependent constitutive relationships. Some material properties in static analyses might be defined as a function of the notional time period, for instance, the shear strain rate in a rate-dependent constitutive model [26,24]. However, the notional time is not real time and the inertial component in Eq. (1) is not considered in the static RITSS approach.

In the dynamic RITSS approach, two additional field variables – the nodal velocities and accelerations – need to be mapped between meshes. The velocities and accelerations at each new element node are interpolated from the deformed old element within which the new node falls

$$\dot{u}_p = N_i\dot{u}_i, \quad \ddot{u}_p = N_i\ddot{u}_i \tag{9}$$

where N_i represents the shape functions of the old element, and $\dot{u}_i$ and u_i are the nodal velocity and acceleration vectors, respectively. The subscript 'p' indicates the projected field variables. The projected velocities and accelerations are transferred into Abaqus/Standard as user-specified initial boundary conditions.

Ideally, the projected field variables, velocities and accelerations at nodes and stresses and material parameters at integration

points, need to be in balance with the external forces and boundary conditions applied on the current geometry at the beginning of each incremental step, since the balance is satisfied naturally at the end of the last step. However, errors induced by projection of the field variables are inevitable, so that the left hand side of Eq. (1) is then marginally divergent from the right hand side at the start of each step:

$$M\ddot{u}_p^{t+\Delta t} + C\dot{u}_p^{t+\Delta t} \approx F_{ext}^{t+\Delta t} - \int_\Omega B^T \sigma_p^{t+\Delta t} d\Omega \tag{10}$$

where B is the strain–displacement matrix and $\sigma_p^{t+\Delta t}$ is the projected stress at time $(t + \Delta t)$. To tackle the unbalance in Eq. (10), an additional numerical small-period time step is set at the commencement of each UL calculation, a new balance thus being achieved. A subsequent question is whether the mapping error is systematically accumulated through multiple steps. It is hard to design a straightforward and theoretically sound test to quantify the error of each step. However, the error is expected to be minimal if the numerical results after frequent mapping do not diverge from known theoretical solutions. The comparisons in terms of three benchmark cases in Section 3 are to demonstrate thoroughly that the error accumulation in the dynamic RITSS is slight.

The detailed procedure for an Abaqus-based dynamic RITSS analysis is shown schematically in Fig. 1. An LDFE analysis is usually composed of 10–3000 steps, so the process has to be performed continually and automatically without the need of any intervention from the user. Therefore, several Python files were coded beforehand to extract the field variables from the result files and to control the mesh regeneration. Python is the script language built into Abaqus [3]. The main program is coded in Fortran, calling Abaqus and the Fortran subroutines that perform the interpolation of the field variables. The main differences between the RITSS approach and decoupled ALE approaches using an explicit scheme, for example Benson [1] and Di et al. [4], are summarized in Table 1.

Although the h-adaptive technique helps to produce an optimal mesh and then improve the numerical accuracy, more effort is then required to calculate the error estimators or error assessors [8]. This technique was not employed in the approach developed. Instead the mesh was generated based on the users' experience and observation of trial calculations based on a coarse mesh.

2.3. Element addition technique

Energy absorbing boundaries have been recognised as crucial to truncate infinite domains in dynamic FE analyses. However, the performance of the absorbing boundary conditions still needs to be assessed carefully when they are used in time-domain problems involving non-linear materials or complex structure-soil interactions [9]. Here a theoretically simple strategy, the element addition technique, is presented for both the static and dynamic analyses using the RITSS approach.

In previous RITSS studies, the Lagrangian FE domain was established prior to the calculation and no more material was allowed to flow into the mesh during the overall analysis. If soil in a given region undergoes extremely large displacements or a long-term dynamic response, the prescribed soil domain has to be sufficient to overcome boundary effects at all times. Even if the far field soil elements stay undeformed during the early steps, these elements are involved in each UL calculation. This drawback is especially severe in dynamic analyses, since the far field boundary should remain sufficiently distant from the structural element to prevent, or at least minimize, the influence of wave reflections.

The element addition technique is therefore used to reduce the computational effort as well as enhancing the accuracy. This technique is particularly appropriate for problems that involve large monotonic displacements. For example, the run-out distance of a submarine debris slide can reach the order of 100 km [11]. When the element addition technique is utilised, the downstream seabed soil is taken into consideration only when this enters the zone of influence of the debris. The element addition technique is performed using the following procedure:

(1) When the far field zone is disturbed by a threshold amount, the problem domain is enlarged at this face, which corresponds to the direction of the structural movement or the sliding soil. The new domain is then remeshed at the beginning of the next increment.
(2) The corresponding old boundary conditions are replaced by the new ones set at the edges of the attached zone. Since the attached zone is unaffected by the preceding response, the integration points located in this zone are assigned intact material properties and geostatic initial stresses. The initial velocities and accelerations in this zone are taken as zero for dynamic analyses. The old boundary conditions are then released. The old boundaries are far away from the zone of concern and the old boundary elements are supported by the newly attached elements, so that the computational accuracy is only slightly affected – as demonstrated in the benchmark examples by the smoothness of the response on either side of the element addition step.
(3) The choice of when to perform element addition depends on a combination of several factors, such as the material properties, distances between the structure and boundaries and velocity of the moving structure or soil. Since the initial

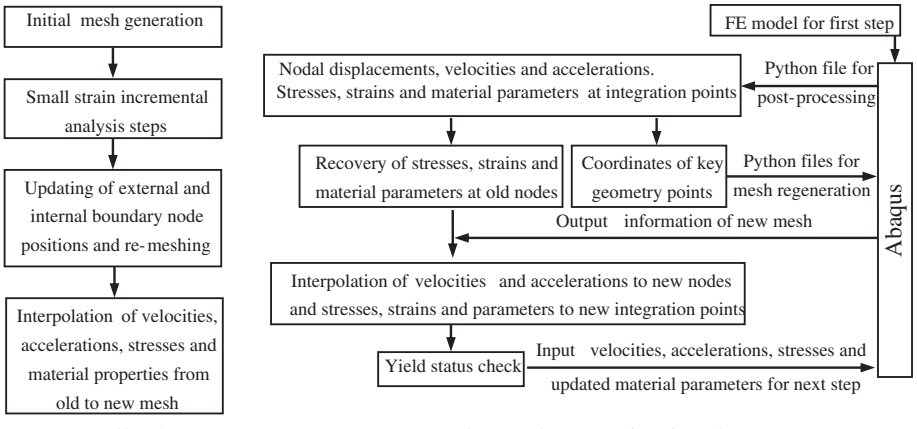

Fig. 1. Procedure of Abaqus-based dynamic RITSS large deformation analysis.

Table 1
Comparison between the RITSS and decoupled ALE using an explicit scheme.

	RITSS	Decoupled ALE using an explicit scheme
Time integration scheme	Implicit	Explicit
Order of elements	Quadratic	Linear
Topology of mesh	Changeable	Unchanged
Projection operation	Locally (in element patch or element)	Globally in FE region
Computational cost	Mainly on UL calculations. Cost of projection is negligible	High efficiency of Lagrangian phase, but the convection is more expensive than that in the RITSS approach

stresses induced by soil self weight have to be considered in most geotechnical problems, a change relative to the initial stresses can be used to determine when to extend the domain boundaries. The criterion explored here was for element addition to be applied once the initial vertical or horizontal stress at any integration points located near the extendable boundaries changed by more than 5%.

In dynamic LDFE analyses, a further criterion arises from the nodal velocities near the movable boundaries. The transmission of dynamic waves in the soil gradually mobilizes the far-field soil from the initial at-rest state, even if the changes relative to the geostatic stresses are minimal. In parallel with the stress change limit, the second criterion was that if the magnitude of the nodal acceleration exceeds a threshold value, the FE domain is extended. The threshold acceleration was adopted as $(\dot{u}^{t+\Delta t} - \dot{u}^{t})/\Delta t > 0.02g$, g representing gravitational acceleration.

In any particular application, it is recommended that a conventional LDFE analysis is first performed without element addition, using a relatively coarse mesh, to select the critical thresholds to avoid boundary effects. Once one of these limits is triggered during a remeshing step, new soil zones are added into the subsequent Lagrangian step according to specifications prescribed in the Python file.

3. Numerical examples

The dynamic RITSS approach is validated through three large deformation benchmark problems, by comparison with two other LDFE approaches and analytical estimations. The first case studies the dynamic response of a shallow footing placed on clay, the second explores a stiff, non-deforming block sliding along soft clay and the third mimics soft clay sliding along the surface of a stronger seabed. In all cases, the soil is meshed with quadratic triangular elements and is assumed to deform under undrained conditions, with a reference strength profile described as

$$s_u = s_{um} + kz \tag{11}$$

where s_{um} is the shear strength at the mudline, k is the strength gradient and z is the soil depth. The clay was modelled as an elastic-perfectly plastic material obeying the Tresca yield criterion. Poisson's ratio was taken as 0.49 to approximate constant volume conditions. Young's modulus is taken as $E = 100s_u$ in the first case (following [12]) and $E = 500s_u$ in the second and third cases. No material damping was incorporated into the numerical simulations. The gravitational acceleration is taken as $g = 10\ m/s^2$ as considering self weight of soil.

A possible application of the dynamic LDFE analysis is to assess the geohazard caused by submarine landslides. For instance, debris flow from a submarine slide may impact on pipelines lying on the seabed surface. The resulting force on the pipeline will depend on the velocity and soil strengths within the debris flow [25]. The last two cases were therefore designed to highlight the potential of the dynamic RITSS approach in landslide simulation.

3.1. Footing under dynamic loads

The mapping of the field variables and possible error accumulation in the dynamic RITSS strategy are assessed in this case by direct comparison of the same boundary value problem tackled using an ALE approach, as reported by Nazem et al. [12]. A strip footing with width of 1 m is placed on weightless uniform clay. The footing-soil interface is fully rough. The density and undrained strength of soil are $\rho = 1000\ kg/m^3$ and $s_u = 1$ kPa. The pressure load, q, is applied to the footing at a constant rapid rate of $20s_u/s$ and a slow rate of $2s_u/s$, respectively. The soil mesh prior to loading is shown in Fig. 2a, with only half of the footing being taken into consideration due to geometric symmetry. The width of the half footing, B, is 0.5 m.

To eliminate the influence of mesh density in this comparison, the characteristic sizes of the soil elements underneath the footing and around the footing corner are ~0.25B, similar to those used by Nazem et al. [12]. The element addition technique is not implemented in the case. Instead, the horizontal and vertical extents of the soil domain are fixed at 50B and 40B respectively. From trials using different mesh extents, these values are sufficiently large for the adopted loading periods. A typical mesh regenerated during the fast loading process is shown in Fig. 2b, in which the footing settlement is $w = 2B$. Clearly, all elements remain well-shaped through periodic remeshing.

The normalised relationships between applied pressure and footing settlement are plotted in Fig. 3. The curves from the RITSS and ALE approaches achieve excellent agreement, regardless of whether the pressure is applied rapidly or slowly. For the strip shallow footing under static pressure, the exact solution of bearing capacity factor is $N_c = q/s_u = 5.14$. The static resistance is enhanced with the footing settlement, with capacity factor reaching 7.28 at settlement of $w/2B = 1.2$ based on the static RITSS analysis. In dynamic large deformation analyses, the resistance, expressed as q/s_u at settlement of $w/2B = 1.2$ is increased to 19.13 for the fast rate and 9.35 for the slow rate, due to inertial effects. The corresponding velocities of footings at $w/2B = 1.2$ are ~3.5 m/s and 1.2 m/s, respectively. Nazem et al. [12] noted that their ALE approach, when running at the slow rate, lost convergence and stopped abruptly when the pressure was increased to $q/s_u = 8.52$. In contrast, the dynamic RITSS approach shows sound numerical stability. There was no occurrence of non-convergence during the entire loading process (see Fig. 3).

The cycle of 'UL calculation – mesh generation – projection' was repeated 36 times for the fast load case and 14 times for the slow load case, until the footing settlement reached $w/2B = 1.2$. The RITSS analyses, even with such frequent mapping, provided a numerical accuracy comparable with the ALE, suggesting that the projection operation developed is reliable. It is also worth noting that, for comparison purposes, the characteristic element size around the footing was selected deliberately as 0.25B. The dependence of bearing capacity on the mesh density is highlighted in Fig. 4, with the characteristic element size around the footing taken as 0.25B, 0.1B and 0.067B. In terms of both fast and slow loading

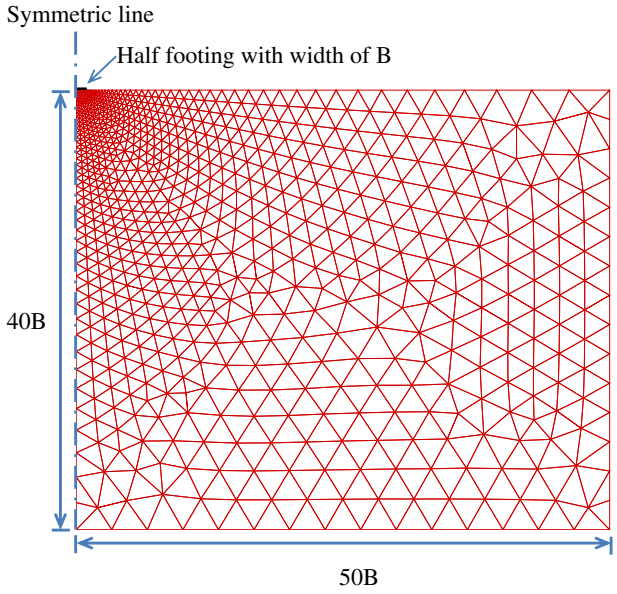

(a) Initial mesh of the whole soil region

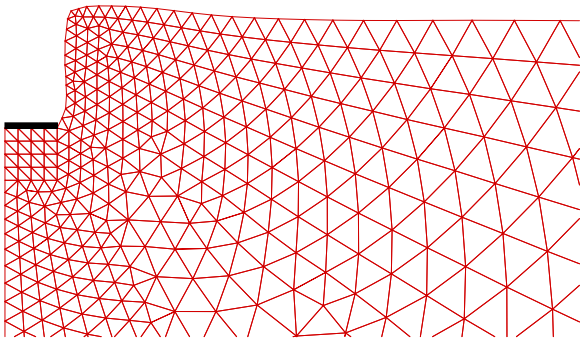

(b)Mesh after footing settlement of 2B under fast loading

Fig. 2. Mesh regeneration during dynamic RITSS analysis.

rates, the bearing capacity is reduced marginally as the characteristic element size is reduced from 0.25B to 0.1B, but the capacity is almost independent of the element size below 0.1B.

3.2. Rigid block sliding on soft clay

The second validation case is an analysis of an (artificially) rigid submarine landslide, moving along a gently inclined deformable

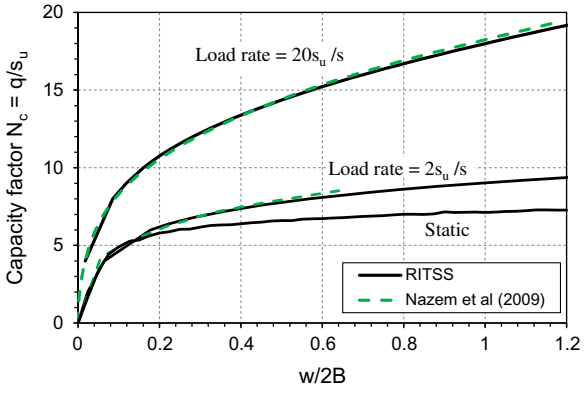

Fig. 3. Normalised footing load–displacement curves under dynamic loads.

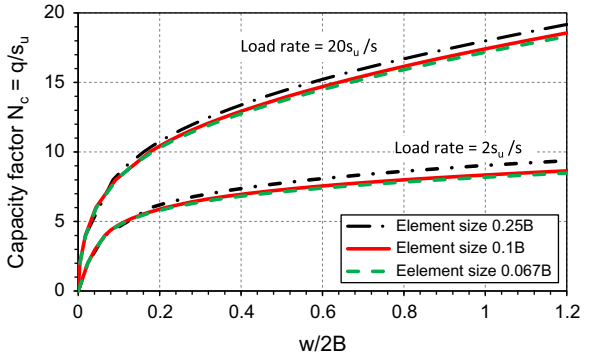

Fig. 4. Effect of mesh density (all curves obtained using the RITSS approach).

seabed as shown schematically in Fig. 5. A common way to model frictional sliding is to establish a frictional master/slave contact pair. Another option is to replace the contact interface with a thin band of material located between the rigid block and the seabed surface. This second approach was used here, with the material in the thin band treated as a Tresca material but with very low shear strength. The strength of the band governs the maximum shear stress between the block and the seabed soil. It is assumed that the integrity of the rigid block-thin band interface and the thin band-seabed interface is maintained.

The soil strength profile of the clayey seabed is s_{um} = 3 kPa and k = 1 kPa/m. The strength of the thin band is $s_{u,band}$ = 0.3 kPa and the band thickness is taken as 0.5 m. For the slide block, the base width L = 37.32 m, the thickness is 5 m and the area (in elevation) is A_b = 143.3 m^2. The submerged unit weights of the seabed, thin band and rigid block are taken as γ' = 6 kN/m^3. The rigid block runs from an initial velocity of 3 m/s, and the subsequent movement is driven by the self weight. If the seabed inclination is taken as β = 0.746°, the run-out response can be estimated as follows, based on the equilibrium of the slide block:

$$\text{Maximum sliding resistance} = Ls_{u,\text{band}} = 37.32 \times 0.3 = 11.2 \text{ kN/m} \quad (12a)$$

$$\text{Gravitational sliding force} = A_b\gamma' \sin(\beta) = 143.3 \times 6 \times \sin(0.746^\circ) = 11.2 \text{ kN/m} \quad (12b)$$

The particular parameter values have been chosen so that the block may slide down the seabed slope at a constant velocity, equal to the initial value of 3 m/s, if there are no other sources of energy loss.

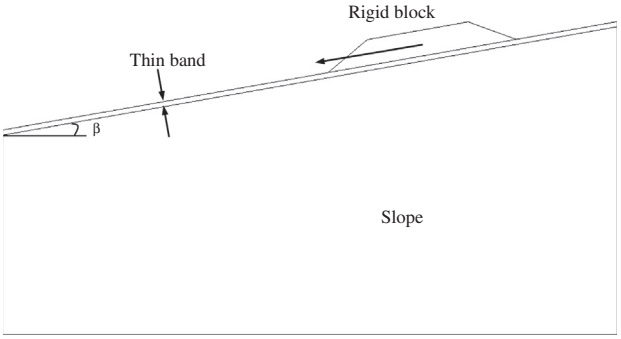

Fig. 5. Problem definition for a rigid block sliding along a submarine slope.

The element addition technique was implemented with a soil zone of horizontal width 10 m being attached to the left boundary at each automatic addition event. The size of the soil elements beneath the slide block is ~0.02L, which was found to be sufficiently fine based on further trials with a finer mesh. Roller constraints were applied on the boundaries of the soil region. The velocity vectors at time $t = 0.1$, 5.9 and 14.8 s are shown in Fig. 6. The rigid block moves leftwards, sliding over the thin band, with the run-out distance reaching 47 m at $t = 14.8$ s. The block does not quite move with a constant velocity (Fig. 7), having an average acceleration of about 0.036 m/s^2 in the period of $t = 0$–14.8 s. This corresponds to a discrepancy in the force balance of 28 %. However, the source of the discrepancy is not wholly numerical rounding and projection errors in the remeshing process. The front toe of the rigid block ploughs into the thin band due to the soil deformation in the band, which causes the 'real' sliding inclination to be slightly larger than the seabed inclination, as the block progressively sinks into the thin weak band (see Fig. 6). For example, the sliding inclination reaches 1.24° at $t = 14.8$ s.

To provide a more clear cut benchmarking case, a further analysis was conducted with the rigid block running along a flat soil surface ($\beta = 0$) and with the gravity loading not applied to the rigid block to diminish the ploughing action into the seabed. The other parameters remained unchanged. The variation of block velocity with time is also plotted in Fig. 7. The velocity decreased with an almost constant deceleration of $a = 0.139$ m/s^2, so the total sliding resistance is

$$A_b \rho' a = 143.3 \times 0.6 \times 0.139 = 11.95 \text{ kN/m} \quad (13)$$

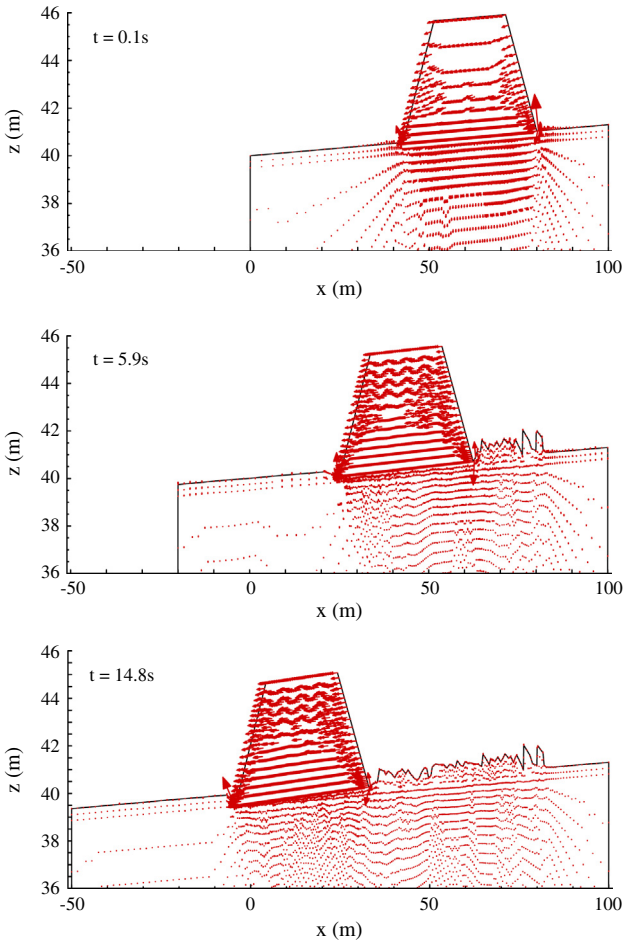

Fig. 6. Instantaneous velocity fields during block sliding (non-scaled geometry).

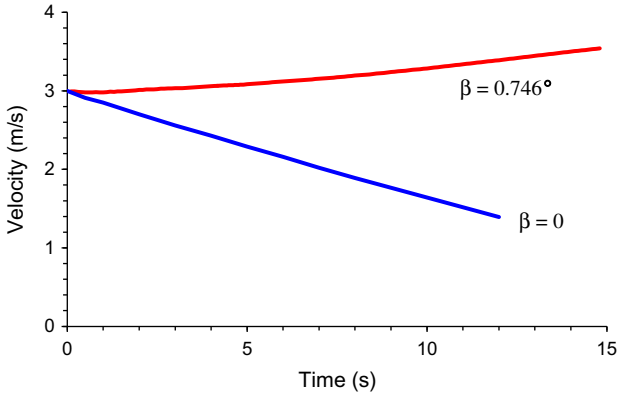

Fig. 7. Velocity history of rigid block sliding.

As mentioned above, the resistance provided by the shear strength of the thin band is 11.2 kN/m, which is only 6.7% lower than the total resistance estimated. Additional resistance may be attributed to the slight ploughing of the block front and the resulting plastic element distortion.

Having demonstrated that dynamic RITSS LDFE analysis can model large submarine slide movements, a potential further application is to explore the evolution of shear strength within submarine landslides, with a view to assessing impact forces on seabed infrastructure such as pipelines. This potential is explored in a different way in the next example.

3.3. Soft clay sliding on rigid surface

The third case is to simulate soft clay sliding along an inclined rigid base using the RITSS approach. Two simulations are shown. Firstly, a comparison is made with the Coupled Eulerian–Lagrangian (CEL) method that is a large deformation approach recently available in Abaqus/Explicit [3]. Secondly, more complex constitutive behaviour is modelled, by incorporating soil softening. This has a dramatic effect on the slide failure mechanism.

In the CEL analysis, an Eulerian mesh is generated to fully cover the deformed soil configuration and the soil materials are allowed to flow in or out of each Eulerian element. The structural elements or stiff seabeds are modelled as Lagrangian bodies. The contact between the Lagrangian body and Eulerian materials is implemented through 'general contact', with the material interfaces being tracked by computing volume fractions of materials within each element. The CEL method was used by Qiu et al. [14] and Tho et al. [17] to investigate quasi-static penetration of the spudcan foundations of jack-up rigs. The computational costs and accuracies of the CEL and the RITSS were quantified and compared for static problems by Tian et al. [18].

The rigid base is fixed with an inclination of 5° and assumed to be fully rough. The initial geometry of the soft clay block is similar to that of the rigid block in Fig. 5, but with base width $L = 48.66$ m. The area of the block is now $A_b = 200$ m^2. The undrained strength of sliding soil is $s_u = 2.5$ kPa and the submerged unit weight is $\gamma' = 6$ kN/m^3. The interaction between the sliding deformable block and the rigid surface is modelled with contact pairs in the RITSS approach. The block is initially stationary and begins to slide due to self weight. The typical element size at the base of the sliding mass is ~0.005L in the analysis using RITSS.

The velocity distributions in the deformed block, predicted by the RITSS approach, are shown in Fig. 8. The soil block is stretched gradually during sliding, with the sliding base along the rigid surface extending. The frictional resistance is thus increased, which decelerates the sliding. This elongation flow mechanism is

accompanied firstly by acceleration of the front toe, then deceleration. The velocity and run-out of the front toe are plotted in Fig. 9. From the RITSS analysis, the velocity increases to a peak value of 4.2 m/s at time $t = 2.8$ s and then reduces to 2.0 m/s at $t = 6$ s and 0.6 m/s at $t = 9$ s. The block front toe becomes essentially stationary at $t = 10.2$ s, indicating a toe run-out distance of 22.8 m. The run-out histories of the front toe derived from the CEL and RITSS analyses agree well with each other. Also, the predicted sliding duration is ~10 s in the CEL analysis and ~10.2 s by the RITSS approach. The run-out distance from the CEL analysis is 21.8 m, only 4.4% lower than that of the RITSS case. The velocity of the front toe is not provided in the CEL analysis, since the nodal variables on the Eulerian mesh such as the velocities and accelerations are not physical values. The RITSS approach shows convincing reliability again in the comparison with the CEL method.

In practice, within a deforming submarine slide the soft clay will be gradually remoulded and softened under the significant deformations occurring within the block. The strain softening behaviour can be modelled by modifying the Tresca model as described by Eq. (14) [29]:

$$s_{us} = [\delta_{rem} + (1 - \delta_{rem})e^{-3\xi/\xi_{95}}]s_u \quad (14)$$

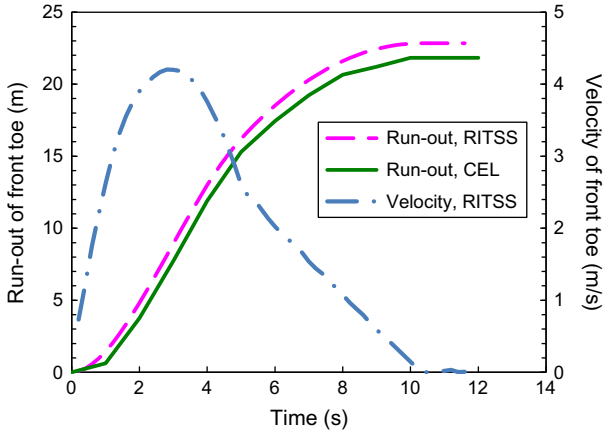

Fig. 9. Run-out and velocity of the front toe.

where δ_{rem} is the ratio between the fully remoulded and initial shear strengths; ξ denotes the accumulated absolute plastic shear strain and ξ_{95} represents the value of ξ at which the soil has undergone 95% of the reduction in strength due to remoulding. In this final

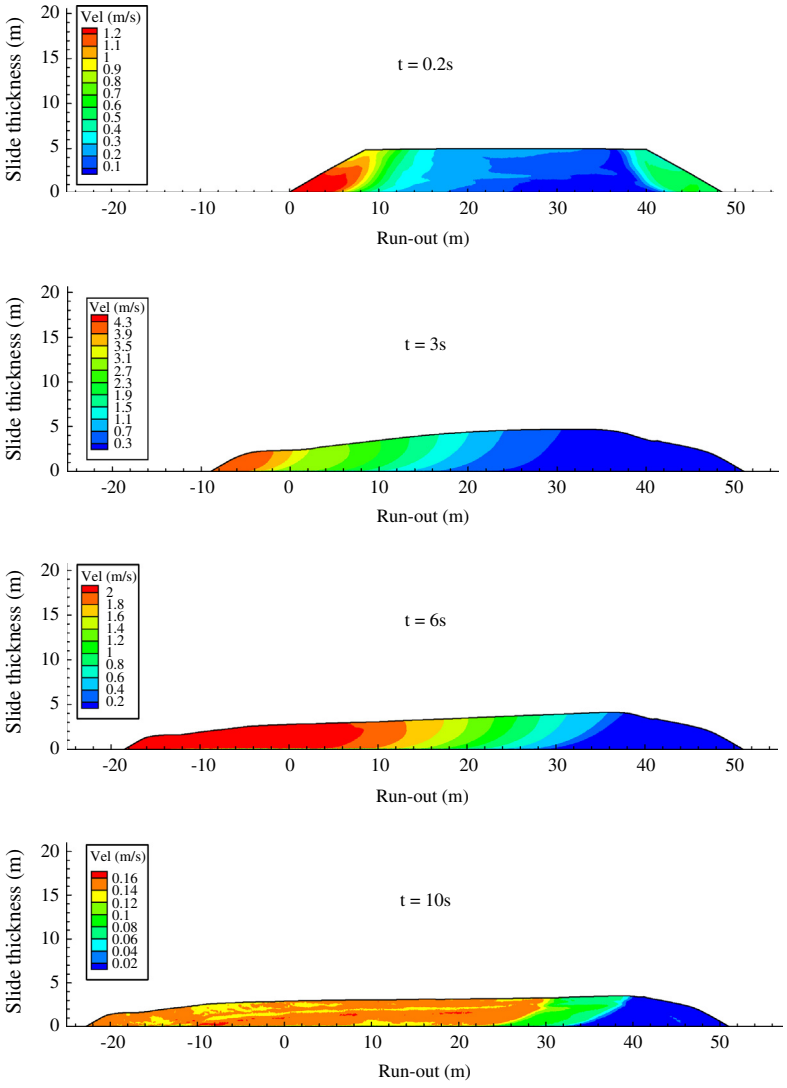

Fig. 8. Velocity distributions within deformed softening block.

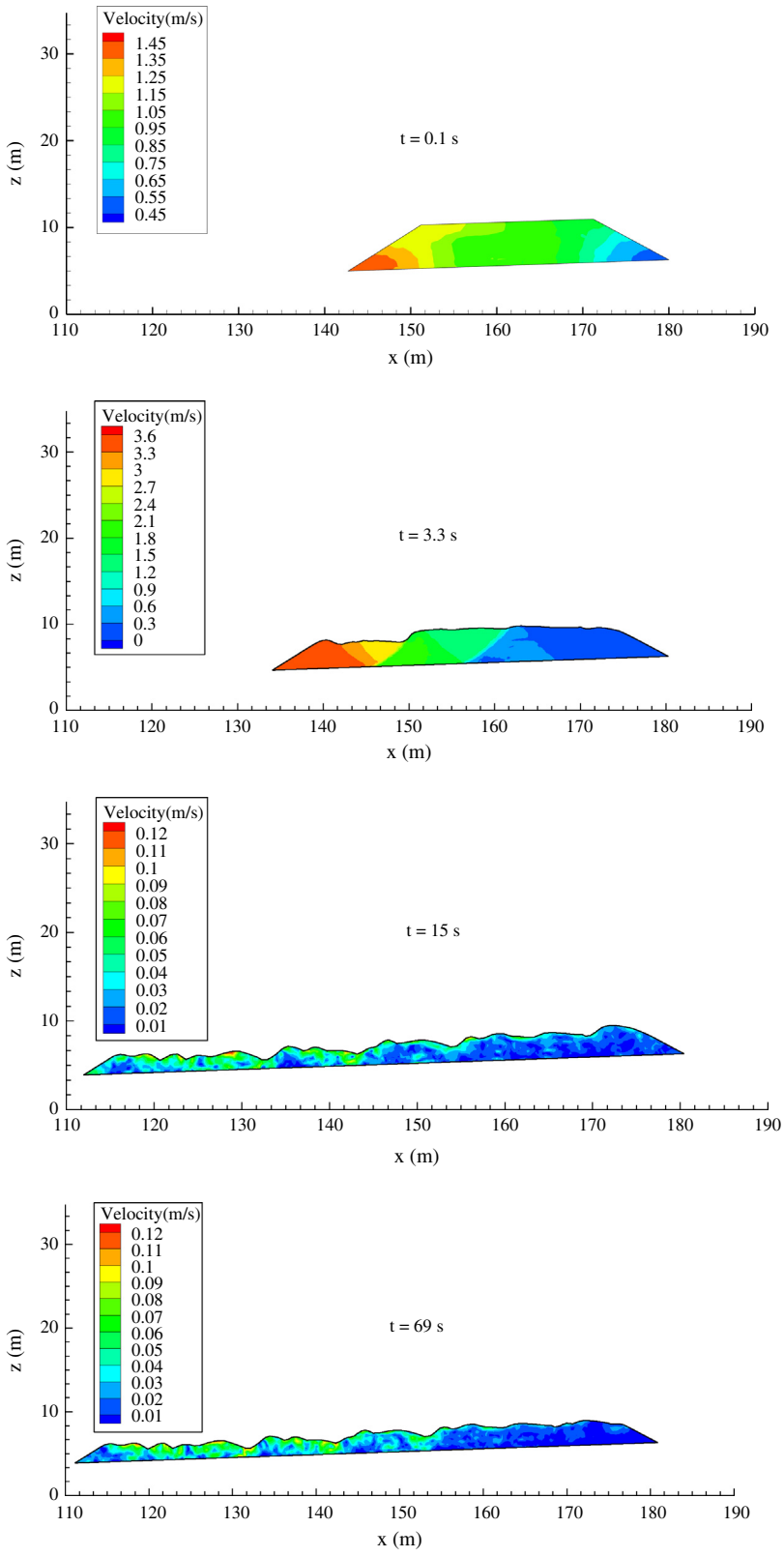

Fig. 10. Velocity distributions in deformed softening block.

demonstration, the intact undrained strength of soft clay is $s_u = 5$ kPa, the softening parameters are $\delta_{rem} = 0.2$ (that is, a sensitivity of 5) and $\xi_{95} = 10$. The soil submerged unit weight is $\gamma' = 6$ kN/m^3. The frictional strength on the seabed-sliding mass interface is taken as 1 kPa and the seabed inclination is $\beta = 2°$. The initial geometry of the soft clay block is similar to the rigid block in Fig. 5. The interaction between the sliding deformable block and the rigid seabed surface is modelled with frictional contact pairs. An initial velocity, $v = 1$ m/s, is imposed on the block, representing the initial soil sliding velocity at some stage following the submarine slide.

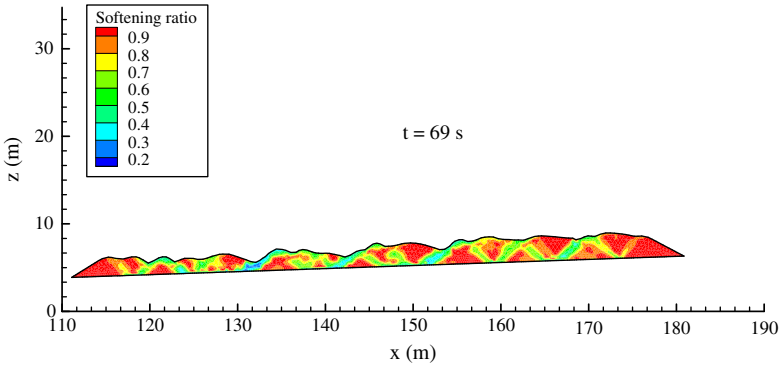

Fig. 11. Soil softening induced within sliding material.

The shape of the deforming block and the internal velocity distributions are shown in Fig. 10. The pattern of internal deformation is dramatically altered compared with Fig. 8. The inclusion of soil softening causes wedges to form at 45 degree inclination, with the shearing becoming concentrated within the weakened soil between the wedges. The sliding base along the seabed surface elongates as the block deforms and correspondingly the frictional resistance continuously increases. The distribution of the softening ratio, s_{us}/s_u, at $t = 69$ s is illustrated in Fig. 11. The pattern of shear band development as the slide material elongates is consistent with the models for retrogressive slide development referred to by Kvalstad et al. [10] and Gauer et al. [5], with a series of triangular wedges separated by fully softened material.

Comparison of Figs. 8 and 10 illustrates the flexibility of this dynamic LDFE technique. The same numerical approach, with minor adjustments of the material properties, can reproduce the behaviour of both highly ductile laminar flows and highly brittle blocky rubbles. This demonstrates the value of this technique as a tool to tackle dynamic large deformation problems in geomechanics.

4. Conclusions

For structure-soil interaction with moderate to high relative velocities, inertial effects must often be considered in addition to large deformations and a changing geometry of the soil domain. A dynamic large deformation finite element (LDFE) approach based on frequent mesh regeneration has been developed for this class of geotechnical applications. In this LDFE approach, an updated Lagrangian calculation is performed in each incremental step; the soil domain is then remeshed and the nodal velocities and acceleration, as well as the stresses and material properties at integration points, are mapped from the old mesh to the new mesh. An element addition technique was incorporated into the LDFE approach to minimize the computational effort by extending the far field boundaries periodically. The technique is valid when the far field soil is in the geostatic state, but would not be valid were the entire domain to be subjected to a ground motion.

The dynamic LDFE approach has been demonstrated in three benchmark cases. The potential application of this method for simulating the long runout of submarine slides has then been illustrated primarily by analysing a block of softening soil, representing part of a submarine landslide, as it moves down a gently sloping seabed of stronger soil. The technique has also been validated against a different technique published previously, by analysing the dynamic embedment of a flat footing.

This technique has many potential applications. It provides a bridge that allows conventional geotechnical continuum finite element techniques to be used in the analysis of problems that have previously been the territory of computational fluid dynamics. This opens up a route for geotechnically-based constitutive models and methods of parameter selection to be applied to problems that have generally been treated using fluid-based constitutive behaviour in the past.

Acknowledgements

The work forms part of the activities of the Centre for Offshore Foundation Systems (COFS), currently supported as a node of the Australian Research Council Centre of Excellence for Geotechnical Science and Engineering. This research is supported by the Australian Research Council through an ARC Discovery Grant (DP120102987) and joint industry project M395 supported by the Minerals and Energy Institute of Western Australia (MERIWA) and six industry sponsors (BP, BHP Billiton, Chevron, Petrobras, Shell and Woodside). The third author acknowledges support from the Shell – EMI partnership at UWA.

References

[1] Benson DJ. An efficient, accurate and simple ALE method for nonlinear finite element programs. Comput Methods Appl Mech Eng 1989;72(3):305–50.
[2] Carter JP, Balaam NP. AFENA User Manual 5.0 1995. Geotechnical Research Centre. Geotechnical Research Centre. Australia: The University of Sydney; 1995.
[3] Dassault Systems. Abaqus Users' Manual; Version 6.10. Providence, R.I.: Dassault Systems Simulia Corp.; 2010.
[4] Di Y, Yang J, Sato T. An operator-split ALE model for large deformation analysis of geomaterials. Int J Numer Anal Meth Geomech 2007;31:1375–99.
[5] Gauer P, Kvalstad TJ, Forsberg CF, Bryn P, Berg K. The last phase of the Storregga Slide: simulation of retrogressive slide dynamics and comparison with slide-scar morphology. Marine Petrol Geol 2005;22:171–8.
[6] Hilber HM, Hughes TJR, Taylor RL. Improved numerical dissipation for time integration algorithms in structural dynamics. Earthquake Eng Struct Dyn 1977;5:283–92.
[7] Hu Y, Randolph MF. A practical numerical approach for large deformation problems in soil. Int J Numer Anal Meth Geomech 1998;22(5):327–50.
[8] Kardani M, Nazem M, Abbo AJ, Sheng D, Sloan SW. Refined h-adaptive finite element procedure for large deformation geotechnical problems. Comput Mech 2012;49(1):21–33.
[9] Kontoe S, Zdravkovic L, Potts DM. An assessment of the domain reduction method as an advanced boundary condition and some pitfalls in the use of conventional absorbing boundaries. Int J Numer Anal Meth Geomech 2009;33(3):309–30.
[10] Kvalstad TJ, Nadim F, Harbitz CB. Deepwater geohazards: geotechnical concerns and solutions. In: Proc offshore tech conf. Houston, Paper OTC 12958; 2001.
[11] Locat J, Lee HJ. Submarine landslides: advances and challenges. Can Geotech J 2002;39:193–212.
[12] Nazem M, Carter JP, Airey DW. Arbitrary Lagrangian–Eulerian method for dynamic analysis of geotechnical problems. Comput Geotech 2009;36:549–57.
[13] Nazem M, Sheng D, Carter JP, Sloan SW. Arbitrary Lagrangian–Eulerian method for large-strain consolidation problems. Int J Numer Anal Meth Geomech 2008;32:1023–50.
[14] Qiu G, Henke S, Grabe J. Application of a Coupled Eulerian–Lagrangian approach on geomechanical problems involving large deformations. Comput Geotech 2011;38(1):30–9.

[15] Randolph MF, Wang D, Zhou H, Hossain MS, Hu Y. Large deformation finite element analysis for offshore applications. In: Keynote Lecture, proc 12th int conf IACMAG, Goa; 2008. p. 3307–18.
[16] Song Z, Hu Y, Randolph MF. Numerical simulation of vertical pullout of plate anchors in clay. J Geotech Geoenviron Eng 2008;134(6):866–75.
[17] Tho KK, Leung CF, Chow YK, Swaddiwudhipong S. Eulerian finite element technique for analysis of jack-up spudcan penetration. Int J Geomech 2012;12(1):64–73.
[18] Tian Y, Wang D, Cassidy MJ. Large deformation finite element analysis of offshore penetration tests. In: Proc 2nd int symp comput geomech, Cavtat-Dubrovnik; 2011. p. 925–933.
[19] Wang D, Gaudin C, Randolph MF. Large deformation finite element analysis investigating the performance of anchor keying flap. Ocean Eng. 2013;59(1):107–16.
[20] Wang D, Hu Y, Randolph MF. Effect of loading rate on the uplift capacity of plate anchors. In: Proc 18th int offshore polar engrg conf, Vancouver, vol. 2; 2008. p. 727–31.
[21] Wang D, Hu Y, Randolph MF. Three-dimensional large deformation finite element analysis of plate anchor in uniform clay. J Geotech Geoenviron Eng 2010;136(2):355–65.
[22] Wang D, Hu Y, Randolph MF. Keying of rectangular plate anchors in normally consolidated clays. J Geotech Geoenviron Eng 2011;137(12):1244–53.
[23] Wang D, Merifield RS, Gaudin C. Uplift behaviour of helical anchors in clay. Can Geotech J 2013;50(6):575–84.
[24] Wang D, White DJ, Randolph MF. Large deformation finite element analysis of pipe penetration and large-amplitude lateral displacement. Can Geotech J 2010;47(8):842–56.
[25] Zakeri A. Review of state-of-the-art: drag forces on submarine pipelines and piles caused by landslide or debris flow impact. J Offshore Mech Arctic Eng 2009;131. Paper 014001.
[26] Zhou H, Randolph MF. Computational techniques and shear band development for cylindrical and spherical penetrometers in strain-softening clay. Int J Geomech 2007;7(4):287–95.
[27] Zhou H, Randolph MF. Resistance of full-flow penetrometers in rate-dependent and strain-softening clay. Géotechnique 2009;59(2):79–86.
[28] Zienkiewicz OC, Zhu JZ. The superconvergent patch recovery and a posterior error estimates. Part 1: The recovery technique. Int J Numer Meth Eng 1993;33:1331–64.
[29] Einav I, Randolph MF. Combining upper bound and strain path methods for evaluating penetration resistance. Int J Numer Meth Eng 2005;63(14):1991–2016.